Characterization of dengue virus 3'UTR RNA binding proteins in mosquitoes reveals that AeStaufen reduces subgenomic flaviviral RNA in saliva

Shih-Chia Yeh[1,*,&], Mayra Diosa-Toro[1,*,¥], Wei-Lian Tan[1], Arthur Hain[1], Celestia Yeo[1], Benjamin Wong[1], Gayathiri Sathiamoorthy Kannan[2], Menchie Manuel[1], Dorothée Missé[3], Yu Keung Mok[2] and Julien Pompon[1,3,¶,Δ]

[1]Programme in Emerging Infectious Diseases, Duke-NUS Medical School, Singapore

[2]Department of Biological Sciences, National University of Singapore, Singapore

[3]MIVEGEC, Univ. Montpellier, IRD, CNRS, Montpellier, France

*Authors contributed equally

¶ Corresponding author: Julien.pompon@ird.fr

Δ Current address: MIVEGEC, Univ. Montpellier, IRD, CNRS, Univ. Montpellier, France

¥ Current address: Department of Biomolecular Health Sciences, Faculty of Veterinary Medicine, Utrecht University, The Netherlands.

& Current address: Cancer Science Institute of Singapore, National University of Singapore, Singapore.

Abstract (300 words)

Dengue viruses (DENV) are expanding global pathogens that are transmitted through the bite of mosquitoes, mostly *Aedes aegypti*. As RNA viruses, DENV rely on RNA-binding proteins (RBPs) to complete their life cycle. Alternatively, RBPs can act as restriction factors that prevent DENV multiplication. While the importance of RBPs is well-supported in humans, there is a dearth of information about their influence on DENV transmission by mosquitoes. Such knowledge could be harnessed to design novel, effective interventions against DENV. Here, we successfully adapted RNA-affinity chromatography coupled with mass spectrometry – a technique initially developed in mammalian cells – to identify RBPs in *Ae. aegypti* cells. We identified fourteen RBPs interacting with DENV serotype 2 3'UTR, which is involved in the viral multiplication and produces subgenomic flaviviral RNA (sfRNA). We validated the RNA affinity results for two RBPs by confirming that AePur binds the 3'UTR, whereas AeStaufen interacts with both 3'UTR and sfRNA. Using *in vivo* functional evaluation, we determined that RBPs like AeRan, AeExoRNase, and AeRNase have pro-viral functions, whereas AeGTPase, AeAtu, and AePur have anti-viral functions in mosquitoes. Furthermore, we showed that human and mosquito Pur homologs have a shared affinity to DENV2 RNA, although the anti-viral effect is specific to the mosquito protein. Importantly, we revealed that AeStaufen mediates a reduction of gRNA and sfRNA copies in several mosquito tissues, including the salivary glands and that AeStaufen-mediated sfRNA reduction diminishes the concentration of transmission-enhancing sfRNA in saliva, thereby revealing AeStaufen's role in DENV transmission. By characterizing the first RBPs that bind to DENV2 3'UTR in mosquitoes, our study unravels new pro- and anti-viral targets for the design of novel

43 therapeutic interventions as well as provides foundation for studying the role of RBPs in virus-
44 vector interactions.
45
46 **Key words:** Dengue transmission, Aedes mosquitoes, RNA-binding proteins, 3'UTR, Staufen,
47 sfRNA, RNA-affinity chromatography.
48
49
50 **Author abstract (150-200 words)**
51 Dengue viruses are important human pathogens transmitted by mosquitoes. Currently, there
52 are no effective control measures for dengue. The RNA-binding proteins (RBPs) in
53 mosquitoes, which bind to the dengue virus genome to regulate viral multiplication, could serve
54 as new targets for developing therapeutic interventions. In this study, we pioneered the use of
55 RNA-affinity chromatography – a technique that identifies proteins binding to specific RNA
56 sequences – in mosquito cells. This led to the detection of fourteen RBPs that bind to the 3'UTR
57 of dengue virus serotype 2. We validated our results using immunoprecipitation method.
58 Furthermore, we demonstrated that 6 of the 14 RBPs influence viral multiplication in
59 mosquitoes. Among these six RBPs, we showed that the AePur mosquito and human homologs
60 share an affinity to dengue virus RNA, whereas the anti-viral function is specific to the
61 mosquito homolog. Importantly, we revealed that AeStaufen mediates a reduction of genomic
62 and subgenomic flaviviral RNAs in multiple mosquito tissues. We also showed that the
63 reduction of subgenomic flaviviral RNA in salivary glands diminishes the secretion of salivary
64 subgenomic RNA, which facilitates infection at the bite site, thereby unveiling the function of
65 AeStaufen in the virus transmission. By characterizing the first mosquito RBPs that bind to

66 dengue virus genome, our study paves the way for leveraging these proteins as potential targets

67 to block virus transmission.

Introduction

Dengue viruses (DENV) are transmitted to humans through mosquito bites, primarily of the *Aedes aegypti* species [1,2]. Given the wide geographic distribution of the mosquito vector and its continuous expansion, almost half of the human population is at risk of infection and about 400 million infections occur every year [3,4]. There are no approved therapeutics for dengue and the only licensed vaccine (DENGVAXIA) has highly variable efficacy against the four DENV serotypes. Moreover, it does not protect against primary infection, considerably limiting its uptake by the population [5]. Broadly-deployed vector control measures based on source reduction and insecticide treatments do not sustainably reduce dengue incidence, even upon sustained and thorough implementation of WHO recommendations [6]. An improved understanding of the molecular interactions that mediate successful viral transmission by mosquitoes is necessary to unravel new targets for the design of effective interventions.

DENV possess a positive-sense single-stranded RNA genome (gRNA) that serves multiple purposes in the viral life cycle. DENV gRNA is translated into viral proteins, functions as a template for RNA replication via the synthesis of complementary negative strands and is assembled into new virions. In all these processes, the gRNA interacts with host RNA-binding proteins (RBPs), which can act as pro or anti-viral factors [7–10]. In humans, several pro-viral RBPs that bind throughout the DENV genome have been identified [11,12]. Furthermore, there is considerable interest in RBPs that interact with the 3'UTR, as the non-coding region is key for viral replication, translation, and assembly [7]. Indeed, DENV replication requires the 3'UTR to interact with pro-viral factors such as polypyrimidine tract-binding protein (PTB), NF90, NFκB2, LSm-1, Dead-box helicase 6 (DDX6), and Exoribonuclease family member 3 (ERI3) [13–18], while its translation and assembly are dependent on 3'UTR binding to two

other pro-viral RBPs, poly-A-binding protein (PABP) [19] and YBX1 [20], respectively. Alternatively, the binding of DENV 3'UTR to Quaking, an anti-viral factor, restricts viral multiplication [21]. All these studies, conducted in human cells, demonstrate the importance of RBPs in DENV cellular cycle. However, there is no information on RBP interaction with the DENV genome or the 3'UTR in mosquitoes.

As in all other flaviviruses, the DENV gRNA is partially degraded by 5'-3' exoribonucleases such as Xrn1 that get stalled at nuclease-resistant structures present in the 3'UTR [22,23]. The abortion of the RNA decay process leaves a highly structured RNA fragment, corresponding to a partial 3'UTR sequence, referred to as subgenomic flaviviral RNA (sfRNA). DENV sfRNA is known to function as an immuno-suppressor via its interaction with several RBPs [24]. In humans, DENV sfRNA interacts with TRIM25 to inhibit signaling of the anti-viral interferon pathway [25] and with G3BP1, G3BP2, and Caprin1 to downregulate the translation of interferon-stimulated genes (ISG) [26]. In mosquitoes, DENV sfRNA inhibits the expression of components of the Toll immune pathway to promote viral transmission [27]. Furthermore, we recently revealed a new function for sfRNA at the interphase between mosquitoes and humans. We showed that sfRNA is secreted in mosquito salivary vesicles to enhance saliva-mediated infectivity in human skin cells and promote infection at the bite site [28]. The multiple functions of sfRNA in viral transmission has accentuated interest in identifying RBPs that bind to DENV 3'UTR in mosquitoes.

In this study, we aim to identify RBPs that bind to DENV 3'UTR in mosquitoes and to characterize their functions in DENV transmission. Using RNA-affinity chromatography coupled with quantitative mass spectrometry (MS), which was adapted from earlier studies on RBP-3'UTR interactions in human cells [18,21,25], we identified fourteen proteins that interact

with the 3'UTR of DENV serotype 2 (DENV2) in *Ae. aegypti* cells. We validated these findings by confirming that AePurine-rich element binding protein (AePur) binds the genomic 3'UTR, whereas AeStaufen interacts with both 3'UTR and sfRNA. We then documented the effects of the fourteen proteins on *in vivo* mosquito infection, which revealed pro-viral functions for three RBPs (AeRan and two nucleases) and anti-viral functions for two other proteins (GTPase and AePur). We found that while AePur 3'UTR interaction is conserved in the human homologs, the anti-viral function is specific to the mosquito protein. Finally, we discovered that AeStaufen reduces both gRNA and sfRNA levels in multiple mosquito tissues, including salivary glands, and that AeStaufen-mediated RNA decay alters the amount of transmission-enhancing sfRNA in the saliva.

Results

Fourteen *A. aegypti* proteins interact with DENV2 3'UTR

To identify proteins interacting with DENV2 3'UTR, we adapted our previously-described approach of RNA-affinity chromatography coupled with mass spectrometry (MS) using mosquito cell lysates (Fig. 1A). We generated a construct containing the T7 promotor, a tobramycin adapter sequence, and DENV2 3'UTR from the NGC strain. For control, we replaced the 3'UTR sequence with a size-matched NS2A gene sequence from DENV2, as previously described [18]. The constructs were transcribed *in vitro* and the RNA sequences were allowed to form secondary structures prior to being incubated with tobramycin-conjugated sepharose beads. The RNA-tobramycin bead conjugates were then incubated with lysates from Aag2 cell line, an *A. aegypti* cell line commonly used for studying anti-viral

136 responses [29]. Eventually, we eluted RNA-bound proteins by adding an excess of tobramycin
137 and quantified them using quantitative MS.

138 Among the 385 proteins detected in the eluates (Table S1), we defined DENV2 3'UTR-
139 interacting proteins as those enriched more than 1.5-fold over the NS2A RNA control, with an
140 adjusted p-value < 0.1. We have identified 14 proteins that met these criteria (Fig. 1B; Table
141 1), which include (in decreasing order of affinity with the viral 3'UTR): AeMaleless, an ATP-
142 dependent helicase involved in dosage compensation [30]; AeSex-lethal, an RNA-binding
143 protein also involved in dosage compensation [31]; an AeGTPase with putative function in
144 translation regulation; AeStaufen, a dsRNA-binding protein that can induce RNA decay and
145 transport [32]; AAEL001518, a protein with no homolog in human and an uncharacterized
146 homolog in *Drosophila melanogaster*; AAEL004834, a putative nucleotide-binding protein;
147 AeRan, a GTPase that is involved in RNA transport [33]; AeDISCO-interacting protein 1
148 (AeDIP1), a dsRNA-binding protein that is involved in antiviral defense [34]; AeRpS24, a
149 ribosomal protein; AAEL014376, an uncharacterized protein; AeRNase, a ribonuclease
150 protein; AeExoRNase, an exonuclease protein with homology to the *Drosophila* RNA-binding
151 protein egalitarian [35]; AeAtu (AeAnother-Translation-Unit), a transcription-regulatory
152 protein [36]; and AePur (AePurine-rich element binding protein), a DNA- and RNA-binding
153 protein [37].

154

155 **Both AePur and AeStaufen interact with DENV2 3'UTR, while AeStaufen also binds**
156 **sfRNA**

157 We were particularly interested in two 3'UTR-interacting proteins, AePur and AeStaufen.
158 Since binding to DENV2 RNA is conserved in the human homolog for AePur [18], the function

159 of this protein could be conserved in both mosquitoes and humans. In the case of AeStaufen,
160 its putative function in RNA decay [32] could modulate the quantity of viral RNA fragments
161 [24]. For these reasons, we validated our RNA-affinity chromatography results with RNA
162 immunoprecipitation (RIP) for AePur and AeStaufen. Pur proteins are a family of single-
163 stranded nucleic acid-binding proteins that are highly conserved from bacteria through humans
164 [38]. Accordingly, we were able to use a commercially available antibody that targets human
165 PurB, to pull down AePur from lysates of orally-infected mosquitoes (Fig. 2A). Using primers
166 that target the envelope gene located in the single open reading frame of DENV gRNA, we
167 observed an enrichment for gRNA (4.59 ± 0.43 fold change) in AePur immunoprecipitates as
168 compared to the IgG control (Fig. 2B). To determine whether AePur binds to gRNA 3'UTR or
169 to sfRNA, both of which have the same sequence, we also quantified sfRNA enrichment as
170 previously described [27]. SfRNA was not enriched in AePur immunoprecipitates as compared
171 to the IgG control (Fig. 2B). Together with the RNA-affinity chromatography results, these
172 data validate AePur interaction with the 3'UTR sequence in DENV2 gRNA.

173 We next tried to confirm AeStaufen binding to DENV2 3'UTR in infected mosquitoes,
174 using the same approach as for AePur. However, attempts to immuno-precipitate AeStaufen
175 using commercially available antibodies developed against its human homolog were
176 unsuccessful. Therefore, we designed an alternative approach that uses C6/36 cells derived
177 from *Aedes albopictus* mosquitoes, which are highly susceptible to DENV infection [39].
178 C6/36 cells were transfected with V5-tagged AeStaufen (Fig. S1) just before infecting them
179 with DENV2. Forty-eight hours post-infection, cell lysates were subjected to RIP using an anti-
180 V5 antibody or IgG control. While the AeStaufen-V5 bands were faint in the pull-downs, there
181 was a clear depletion of the protein in the unbound fractions (Fig. 2C), indicating a moderately

efficient RIP. Nonetheless, DENV gRNA was enriched 9.78 ± 0.61 fold in V5 immunoprecipitates (Fig. 2D). As done in AePur immunoprecipitation, we also determined the affinity of AeStaufen-V5 to sfRNA and observed a lower but significant enrichment (2.69 ± 0.12) for sfRNA in AeStaufen-V5 immuno-precipitates. Together, these results suggest that AeStaufen has a high affinity to gRNA 3'UTR and also interacts with sfRNA. Overall, using RIP experiments, we have validated the 3'UTR-protein interactions identified with the RNA-affinity chromatography and determined the affinity of AePur and AeStaufen for DENV2 3'UTR and sfRNA.

Functional characterization of DENV2 3'UTR-bound proteins in mosquitoes

To test whether the mosquito proteins that bind DENV2 3'UTR influence mosquito infection, we performed *in vivo* dsRNA-mediated silencing for each of the 14 proteins. As control, we injected a dsRNA targeting the bacterial gene *LacZ*. Four days post dsRNA-injection, we validated gene silencing in whole mosquitoes (Fig. S2) and infected mosquitoes by offering a blood meal containing 10^6 DENV pfu/ml, which is within the range of inoculum concentration observed in patient serums [40]. The blood feeding rate was lower only in mosquitoes whose *AeMaleless* and *AePur* genes were silenced, while other silencing had no effect (Fig. S3A).

Seven days post oral infection, we quantified DENV titers in whole mosquitoes using focus forming unit (FFU) assay. As higher infection can reduce mosquito survival [41] and introduce a bias towards the selection of mosquitoes surviving a lower infection, we controlled that survival was similar across the various silencing conditions (Fig. S3B). We then calculated infection rate as the percentage of mosquitoes with at least one viral particle over blood-engorged mosquitoes, and infection intensity as the number of FFUs per infected mosquito.

205 The infection rate provides information about the ability of the virus to initiate infection, while
206 infection intensity is a measure of virus multiplication. Nonetheless, these two biological
207 parameters are interdependent; for instance, reduced viral multiplication (i.e. infection
208 intensity) may lead to viral elimination that would then lower infection rate.

209 In terms of infection rate, we observed that silencing of *AeRan* and *AeExoRNase* reduced
210 the percentage of infected mosquitoes by 23.5 and 29 %, respectively (Fig. 3A), suggesting
211 that these two proteins facilitate infection onset. In terms of infection intensity, four other
212 proteins had an effect (Fig. 3B). *AeRNase* silencing led to a 6.1-fold decrease in the number of
213 FFUs per infected mosquito, indicating its function in facilitating virus multiplication.
214 Inversely, FFUs per infected mosquito increased 10-fold, 15.7-fold and 4.2-fold upon the
215 silencing of *AeGTPase*, *AeAtu* and *AePur*, respectively (Fig. 3B), revealing anti-viral functions
216 for these three proteins. Taken together, this *in vivo* mid-throughput screening provides the
217 first evidence that RBPs influence DENV infection in the mosquito vector.

218

219 **The human homologs of AePur bind DENV gRNA but do not alter infection**

220 In humans, three genes (PURA, PURB, and PURG) encode for four Pur proteins (PurA, PurB
221 and two isoforms of PurG). The highly-conserved purine-rich element binding domain (Pur
222 domain) that is characteristic of Pur proteins and responsible for their interaction with
223 nucleotides [38] is present in both the human and mosquito homologs (Fig. S4). To investigate
224 whether binding to DENV gRNA is conserved between AePur and HsPur proteins, we
225 overexpressed Flag tagged-HsPurA and His-tagged HsPurB in human cells before infecting
226 the cells with DENV2. We chose to study the HsPurA and HsPurB homologs since they are
227 most closely related to AePur (Fig. S4). We used ectopic expression of tagged-proteins as

available antibodies were not suitable for IP. Twenty-four hours post infection, we conducted RIP with either of the tags (Fig. 4A) and quantified gRNA. DENV gRNA was enriched 150 ± 3.8 fold in HsPurA precipitates and 16.6 ± 0.5 fold in HsPurB precipitates as compared to the IgG control (Fig. 4B). A significant part of the overexpressed proteins remained in the unbound fractions (Fig. 4A), suggesting that gRNA-protein interactions were underestimated. These results show that binding to the DENV genome is conserved across Pur homologs in both humans and mosquitoes.

We next tested if human Pur proteins influenced DENV2 infection. We separately depleted either HsPurA or HsPurB expression using siRNA-mediated silencing in human cells. To prevent untargeted silencing effects, we used three different siRNA sequences for each of the two Pur proteins and observed specific depletion of either HsPurA or HsPurB (Fig. 4C). The depleted cells were infected with DENV2 and viral titer was quantified using plaque forming unit (PFU) assay 24h later. There was no effect of either HsPURA or HsPURB silencing on viral titer as compared to non-transfected (NT) and siRNA-transfected controls (siNC) (Fig. 4D). To rule out the possibility that background levels of the HsPur proteins and/or functional redundancy between HsPurA and HsPurB could be responsible for unaffected DENV titers, we generated cells devoid of both HsPurA and HsPurB via CRISPR/Cas9 editing. To prevent untargeted effects of the knock-out approach, we produced four different cell lines in which both HsPurA and HsPurB expressions were abrogated (Fig. 4E). Similar to the silencing approach (Fig. 4D), DENV titers remained unaffected in the absence of both HsPur proteins (Fig. 4F). Altogether, these results indicate that HsPurA and HsPurB strongly interact with DENV2 gRNA like AePur. However, the anti-viral function of AePur is not conserved in the human homologs.

AeStaufen reduces gRNA and sfRNA quantities in mosquito carcass, midgut and salivary glands but does not affect viral titer

To functionally characterize AeStaufen, we first quantified its relative expression under non-infected and infected conditions in whole mosquito, midgut, salivary glands, and carcass (remains of midgut and salivary glands dissection). *AeStaufen* expression was normalized to that of *Actin* for comparison among the tissues. While *AeStaufen* expression was not affected by oral infection within each of the tissues, salivary glands had the highest *AeStaufen* expression among the tissues (Fig. 5A). *AeStaufen* expression was also high in the carcass, suggesting that organs remaining in the carcass, such as ovaries and brain, express high levels of *AeStaufen* as observed in *D. melanogaster* [42]. The expression pattern of *AeStaufen* indicates its ubiquitous presence, with important functions in certain tissues, such as the salivary glands, where it is most expressed.

To evaluate the effect of AeStaufen on DENV2 infection in the carcass, midgut and salivary glands, we silenced *AeStaufen* by injecting a large quantity of dsRNA that is sufficient to decrease mRNA levels across the mosquito organs (Fig. S5). A similar amount of *dsLacZ* was injected as control. The mosquitoes were orally infected at four days post-dsRNA injection, and gRNA was quantified at 10 days post-oral infection (dpi) in the carcass, midgut and salivary glands. To exclude bias caused by enhanced survival of less-infected mosquitoes, we controlled that blood feeding and survival rates were not affected by AeStaufen depletion (Table S2). Similar to FFU quantification described above, we calculated infection rate as the percentage of tissues with at least one gRNA and infection intensity as the number of gRNA copies per infected tissue. Infection rates in all the tissues were unaffected by *AeStaufen*

274 silencing, suggesting that AeStaufen does not influence infection onset (Fig. 5B). However,
275 infection intensity increased 3.02-fold and 5.67-fold upon AeStaufen depletion in the carcass
276 and salivary glands, respectively (Fig. 5B). It is interesting to note that these tissues exhibited
277 highest *AeStaufen* expression (Fig. 5A). In the midgut, AeStaufen depletion led to a 3.61-fold
278 increase in infection intensity (Fig. 5B), although the difference was not statistically significant
279 ($p = 0.12$, as determined by t-test). These results reveal that AeStaufen mediates reduction in
280 DENV gRNA copies in multiple organs of mosquitoes.

281 Since AeStaufen also interacts with DENV2 sfRNA (Fig. 2D), we then determined the
282 effect of AeStaufen depletion on sfRNA copies in the same samples. We calculated the sfRNA
283 detection rate to inform about the initiation of sfRNA production, and the sfRNA copies per
284 infected tissue to evaluate the effect on the production and/or degradation of sfRNA. While
285 AeStaufen depletion did not change sfRNA detection rate, it increased sfRNA copies per
286 infected tissue by 6-fold, 14.43-fold, and 10.99-fold in the carcass, midgut, and salivary glands,
287 respectively (Fig. 5C). To normalize sfRNA quantity to the amount of its precursor and the
288 level of infection (both determined by gRNA), we calculated the sfRNA:gRNA ratio.
289 AeStaufen depletion increased the sfRNA:gRNA ratio only in the midgut and salivary glands,
290 by 2.19-fold and 2.47-fold, respectively (Fig. 5D). Altogether, these results indicate that
291 AeStaufen mediates decrease in both gRNA and sfRNA copies in all tissues, but that its effect
292 on sfRNA is more pronounced in the midgut and salivary glands.

293 We have previously shown that DENV2 strains producing higher sfRNA copies in the
294 salivary glands result in a higher viral titer in the tissue and a higher saliva-mediated infection
295 rate [27]. To test whether higher sfRNA:gRNA ratio in the salivary glands resulting from
296 AeStaufen depletion reproduces these observations, we quantified viral titers in the salivary

297 glands and saliva of AeStaufen-depleted mosquitoes. To exclude bias caused by unsalivating
298 mosquitoes, we controlled that the salivation rate was not affected by *AeStaufen* silencing
299 (Table S2). Both infection rate and infection intensity were unaffected by AeStaufen depletion
300 in the salivary glands and saliva (Fig. 5E, F). Together with the lack of effect on infection in
301 AeStaufen-depleted mosquitoes (Fig. 3), these results indicate that AeStaufen does not alter
302 the production of infectious viral particles.
303
304 **AeStaufen reduces the amount of sfRNA secreted in saliva**
305 Our group had previously demonstrated that DENV secretes the anti-immune sfRNA in
306 mosquito saliva to enhance saliva infectivity in human skin cells, thereby increasing viral
307 transmission [28]. To determine whether AeStaufen's effect on sfRNA and gRNA in the
308 salivary glands modifies the sfRNA:gRNA ratio in the saliva, we quantified gRNA and sfRNA
309 in AeStaufen-depleted mosquito saliva at 10 dpi. gRNA detection rate and gRNA copies per
310 infected saliva were very similar in AeStaufen-depleted and control mosquitoes (Fig. 6A).
311 Inversely, sfRNA:gRNA ratio increased 1.89-fold upon AeStaufen depletion, although sfRNA
312 detection rate was unaltered (Fig. 6B).
313 We next tested whether the increase in sfRNA:gRNA ratio in the saliva was caused by
314 AeStaufen-mediated sfRNA degradation in the salivary glands. To infect salivary glands
315 without going through midgut infection, we inoculated AeStaufen-depleted mosquitoes and
316 quantified gRNA and sfRNA in salivary glands at 7 days post inoculation. gRNA detection
317 rate ($p = 0.10$, as determined by Z-test) and gRNA copies per infected salivary glands were not
318 altered (Fig. 6C). However, similarly to what we observed in salivary glands from orally-
319 infected mosquitoes, sfRNA:gRNA ratio was increased 1.77-fold in salivary glands from

320 inoculated mosquitoes (Fig. 6D). Altogether, these results indicate that AeStaufen-mediated
321 reduction of sfRNA quantity in salivary glands influences the ratio of sfRNA:gRNA in saliva.
322
323 **Discussion**
324 While the importance of RBPs in DENV life cycle is well-supported in mammals [7], there is
325 a dearth of knowledge about RBP identities and functions in mosquitoes. By successfully
326 pioneering the use of RNA-affinity chromatography in mosquito cells, we discovered fourteen
327 mosquito RBPs that interact with DENV2 3'UTR in *A. aegypti*. Furthermore, using *in vivo*
328 functional analyses, we determined that three RBPs have pro-viral functions and three others
329 have anti-viral functions. We then evaluated the affinities of two RBPs, AePur amd AeStaufen,
330 for either 3'UTR or sfRNA (as both share the same sequence), concomitantly validating the
331 RNA-affinity chromatography results. AePur interacts specifically with the 3'UTR, whereas
332 AeStaufen binds both 3'UTR and sfRNA. We further showed that the affinity for DENV RNA
333 is conserved across AePur homologs, although only the mosquito homolog has anti-viral
334 functions. Importantly, we revealed that AeStaufen mediates reduction of gRNA in the carcass
335 and salivary glands, and of sfRNA in the carcass, midgut, and salivary glands. While
336 AeStaufen-mediated decay of viral RNA does not influence the number of infectious viral
337 particles, it reduces the concentration of transmission-enhancing sfRNA in the saliva, revealing
338 AeStaufen impact on viral transmission. By characterizing the first DENV RBPs in mosquitoes,
339 this study unravels their multipronged functions in DENV transmission.
340 Interestingly, the binding affinity to DENV RNA is conserved in the human homologs of
341 eight of the 14 RBPs we identified in mosquitoes (Table 1). A Comprehensive identification
342 of RNA-binding proteins by mass spectrometry (ChIRP-MS) study in human cells found that

DHX9, DHX29, DHX36, and DHX57 (homologs of AeMaleless) and ELAVL1 (AeSex lethal homolog) interact with DENV2 and Zika virus genomes [11]. However, an RNA-affinity chromatography approach (similar to the one used in this study) found that DHX9 has less affinity to the 3'UTR of DENV1-4 than to a control RNA fragment, while DHX36 only marginally (1.30-fold) interacts with DENV2 3'UTR [43]. These contrasting results for genomic RNA and 3'UTR binding suggest that the RBPs preferentially interact with sequences outside the 3'UTR in human cells. Furthermore, Staufen 1 (AeStaufen homolog) binds DENV2 and Zika virus gRNA [11] but not the 3'UTR of DENV1-4 [21]. Ran (AeRan homolog) interacts with a concatenated sequence of DENV2 5'UTR and 3'UTR as identified by RNA-affinity chromatography [18], and with the DENV2 genome as identified by ChIRP-MS [11]. RPP14 (AeRNase homolog) and LEOA (AeAtu homolog) interact with DENV2 3'UTR [21], while PURB (AePur homolog) binds the concatenated sequence of 5' and 3'UTRs [18]. The conservation of RBP affinity for DENV RNA across human and mosquito homologs suggests that the virus has evolved to exploit the biological similarities between its two hosts.

We have identified six RBPs that influence DENV infection in mosquitoes. We found that AeRan, a small GTPase, favors DENV infection by promoting the infection rate. Its human homolog, Ran, has a well-supported function in the nucleocytoplasmic transport of RNA [44]. Contrary to its pro-DENV effect in mosquitoes, *D. melanogaster* Ran contributes to anti-viral immune response by regulating virus phagocytosis and enabling the nuclear translocation of transcription factors activated by the Toll signaling pathway [45,46]. We also found that AeExoRNase (a predicted exoribonuclease) is required for optimal infection rate in mosquitoes. Its *Drosophila* homolog, egalitarian, has RNA-binding capacity and is involved in RNA localization [47,48], suggesting that AeExoRNase is required for proper DENV gRNA

366 transport. Moreover, we observed that AeRNase (a subunit of ribonuclease P) enhances
367 infection intensity in mosquitoes, indicating a putative new role for ribonuclease P in virus
368 multiplication. Inversely, an AeGTPase with no functional data for its homologs reduces
369 infection intensity. AeAtu, whose homologs in *D. melanogaster* (i.e. Atu) and humans (i.e.
370 LEO1) are involved in gene regulation [36], had the strongest anti-viral impact. LEO1 is a
371 component of Polymerase Associated Factor 1 complex (PAF1C), which mediates a strong
372 anti-viral response through gene regulation [49]. Although AeAtu function in mosquitoes is
373 unknown, it is tempting to speculate that the PAF1C immune regulation is conserved in
374 mosquitoes. Finally, we noted that AePur, an RNA- and DNA-binding protein, mediated a
375 reduction in infection intensity. The role of one of the human homologs, PurA, in promoting
376 stress granule formation [50] that is detrimental to viral infection [51] may provide hints on
377 how AePur regulates infection intensity. However, while the binding to DENV RNA was
378 conserved across the human and mosquito Pur homologs, the anti-viral effect was specific to
379 the mosquito protein, indicating functional divergence between the homologs with respect to
380 DENV infection. Together, our mid-throughput *in vivo* screening is the first study to identify
381 RBPs that influence viral multiplication in mosquitoes, and highlights potential new targets for
382 blocking viral transmission.

383 Importantly, we have revealed that AeStaufen mediates a reduction in both DENV gRNA
384 and sfRNA copies. The human and *Drosophila* Staufen homologs bind dsRNA through five
385 dsRNA-binding domains [52], which are conserved in AeStaufen (Fig. S6). SfRNA contains
386 several dsRNA sequences [53] and gRNA possesses multiple hairpins in highly structured
387 regions [54], both of which could allow AeStaufen interaction. Upon binding, Staufen can
388 transport nucleotides to ribonucleoprotein complexes that modulate translation. Alternatively,

389 Staufen can initiate the assembly of an mRNA decay complex, called Staufen-mediated RNA
390 decay (SMD) [32]. Since both its functions are associated with mRNA processing, Staufen is
391 thought to act as post-transcriptional regulator. Therefore, we propose that the increase in
392 gRNA copies that is observed upon AeStaufen depletion results from the inhibition of the SMD
393 pathway in DENV-infected mosquitoes.

394 While several viruses rely on Staufen to complete their life cycles [55–57], this is the first
395 evidence that a Staufen homolog hinders virus multiplication by degrading its gRNA. Another
396 major RNA decay process, called non-mediated RNA decay (NMD), was previously shown to
397 degrade viral RNA and reduce viral titer [58]. However, in our study, the increase in gRNA
398 copies upon AeStaufen depletion did not translate into higher number of infectious particles in
399 both whole mosquitoes and salivary glands. Such discrepancy between gRNA copies and
400 virion number suggests that the cellular localization of gRNA that is degraded is different from
401 that of the gRNA that is assembled in virions. Positive-sense gRNA is produced in replication
402 complexes located at the endoplasmic reticulum (ER) and is then assembled at a distinct ER
403 assembly site [7,59]. The translocation of newly-synthesized viral RNAs from the replication
404 to assembly site is aided by viral and host cellular RBPs [59,60] Nevertheless, AeStaufen may
405 be degrading gRNA that is not directed to the assembly sites, but is instead transported to other
406 cellular compartments. Staufen is usually found in stress granules, where the SMD machinery
407 is assembled [61]. We hypothesize that the gRNA molecules that are not directed towards
408 virion production sites are released actively or passively from the replication complexes, where
409 they are degraded by an AeStaufen-mediated mechanism.

410 SfRNA, which is derived from gRNA degradation, was increased upon AeStaufen
411 depletion in the carcass, midgut and salivary glands. Increased sfRNA production could result

412 from a higher quantity and availability of its gRNA template. In this case, higher gRNA copies
413 as reported in carcass and SG would proportionally increase sfRNA copies independently of
414 AeStaufen. To inform about a proportional relationship between sfRNA and gRNA quantities,
415 we calculated sfRNA:gRNA ratio. In the carcass, the ratio was unchanged by AeStaufen
416 depletion, suggesting that a higher gRNA copies led to increased production of sfRNA.
417 However, higher sfRNA:gRNA ratios in AeStaufen-depleted midgut and salivary glands imply
418 that gRNA and sfRNA quantities are uncoupled (ie., sfRNA copies are not solely dependent
419 on gRNA copies). Together with the binding of AeStaufen to sfRNA, the results indicate that
420 AeStaufen mediates sfRNA degradation in the midgut and salivary glands.

421 SfRNA has multipronged functions in viral transmission [24]. We had previously reported
422 that higher sfRNA concentration in the salivary glands increases virion quantity by inhibiting
423 the Toll immune pathway [27]. Surprisingly, a higher sfRNA concentration in the salivary
424 glands induced by AeStaufen depletion did not result in increased virus titer in the salivary
425 glands and saliva. As for gRNA, this may stem from different cellular localizations of the
426 sfRNA molecules degraded via AeStaufen and the sfRNA molecules involved in regulating
427 immunity. The Toll pathway components are localized in plasma membrane or cytosol [62],
428 whereas SMD complexes are localized in stress granules [61]. We also previously reported that
429 sfRNA is secreted in salivary extracellular vesicles to enhance infection at the bite site [28].
430 Here, we have shown that AeStaufen-mediated reduction of sfRNA takes place in the salivary
431 glands and that this reduces the quantity of secreted sfRNA. Altogether, these results show that
432 AeStaufen regulates viral transmission by modulating salivary sfRNA concentrations.

433 In conclusion, our successful adaptation of a biochemical technique employed in
434 mammals has led to the identification of multiple mosquito RBPs that bind to DENV RNA and

435 modulate its life cycle. Since several of these RBPs have roles in viral multiplication, they
436 could be used as potential targets for the design of novel, effective interventions for dengue
437 prevention. Furthermore, by describing the effects of AeStaufen on DENV gRNA and sfRNA
438 levels, we have unraveled a new role for AeStaufen in viral transmission by mosquitoes. Our
439 identification of the multiple ways RBPs can regulate DENV transmission motivate further
440 studies of RBPs in mosquitoes.
441

Materials and Methods

Cell lines, virus, and mosquitoes

Aedes albopictus C6/36 (CRL-1660) and baby hamster kidney BHK-21 (CCL-10) cell lines obtained from ATCC, and *Aedes aegypti* Aag2 cells received from Dorothée Missé's lab were grown in Roswell Park Memorial Institute medium (RPMI, Gibco). Human hepatic Huh7 cells (JCRB0403) were maintained in Dulbecco's Modified Eagle Medium (DMEM, Gibco). For all cell lines, the medium was supplemented with 10 % heat-inactivated fetal bovine serum (FBS) (ThermoFisher Scientific), 100 U/ml penicillin, and 100 µg/ml streptomycin (ThermoFisher Scientific). Mosquito cells were cultured at 28 °C with 5 % CO_2, and mammalian cells were grown at 37 °C with 5 % CO_2.

Dengue virus 2 (DENV2) New Guinea C (NGC) strain from ATCC (VR-1584) was propagated in C6/36 cells and titrated using plaque assay (this determines the number of plaque forming units, pfu) in BHK-21 as previously detailed (1).

The *Aedes aegypti* colony was established from eggs collected in Singapore in 2010 and reared in the insectary thereafter. The eggs were hatched in MilliQ water and the larvae were kept at a density of 2.5-3 larvae/cm^2 in shallow water and fed on a mixture of TetraMin fish flakes (Tetra), yeast, and liver powder (MP Biomedicals). Adult mosquitoes were maintained in a 30×30×30 cm cage (Bioquip) and fed with 10% sucrose solution (1st base) *ad libitum*. They were maintained at 28°C and 50% relative humidity in a 12h:12h light: dark cycle.

RNA-affinity chromatography

The method was modified from (2) except that the Stable Isotope Labeling with Amino acids in Cell culture (SILAC) technique was not used. In brief, DENV2 3'UTR and size-matched

NS2 control templates were amplified from viral cDNA using AW005 5'-CGGGTATGTGCGTCTGGATCCTATAAGAAGAGGAAGAGGCAGG-3' and AW043 5'-AGAACCTGTTGATTCAACAGCAC-3', and AW024 5'-CGGGTATGTGCGTCTGGATCCTATGCAGCTGGACTACTCTTGAG-3' and AW047 5'-GGTCCTGTCATGGGAATGTC-3', respectively. A T7-flanked tobramycin aptamer was incorporated at the 5'-end of the templates. RNA was generated using MegaScript T7 transcription kit (Invitrogen), folded by heating and subsequent slow cooling, and bound to a tobramycin bead matrix. Beads decorated with 3'UTR or NS2 fragments were incubated with the same amount of pre-cleared lysate from Aag2 cells. Beads were washed and proteins were eluted along with excess tobramycin using MicroSpin columns (Pierce). The experiment was repeated thrice using different batches of Aag2 cells.

Quantitative Mass Spectrometry

RNA affinity chromatography eluates were analyzed by Data-Dependent Acquisition (DDA) quantitative MS. Trypsin-digested samples were first injected into a trap column (300 µm i.d. x 5 mm, C18 PepMap 100), and then into a C18 reversed-phase home-packed 15 cm column (SB-C18, ZORBAX, 5 micron, Agilent). Flow rate was maintained at 400 nL/min for a 60-min LC gradient, where mobile phase included A (5% ACN, 0.1% FA, Burdick and Jackson) and B (100% ACN, 0.1% FA). The eluted samples were sprayed through a charged emitter tip (PicoTip Emitter, New Objective, 10 ± 1 µm) into Orbitrap Fusion MS system (Thermo Fisher Scientific), coupled with a Dionex Ultimate 3000 nano HPLC (Thermo Fisher Scientific). The following parameters were used: tip voltage at +2.2 kV, FTMS mode for MS acquisition of precursor ions (resolution 120,000), and ITMS mode for subsequent MS/MS of top 10

precursors selected; MS/MS was accomplished via collision-induced dissociation (CID). The Proteome Discoverer 1.4 software was used for protein identification from *A. aegypti* UniProt entries, under the following parameters: maximum missed cleavages = 2; precursor tolerance = 5ppm; MS fragment tolerance = 0.6 Da; peptide charges considered = +2, +3, and +4. The significance of a peptide match was based on expectation values smaller than 0.05. Proteins were considered enriched in 3'UTR when present more than 1.5 fold than in NS2 control sequence with a p-value < 0.1 as determined by t-test after Bonferroni adjustment. The putative functions of the proteins were inferred from functional information available for *Drosophila* and human homologs.

Mosquito oral infection

Three- to five-day-old female mosquitoes were starved for 24 h and offered a blood meal containing 40 % volume of washed erythrocytes from specific-pathogen-free (SPF) pig's blood (PWG Genetics), 5 % of 10 mM ATP (Thermo Fisher Scientific), 5 % of human serum (Sigma) and 50 % of RPMI medium containing DENV2 NGC. A blood viral titer of 10^6 pfu/ml was used for the functional characterization of the 14 proteins interacting with DENV 3'UTR and for AePur RIP. A blood viral titer of 10^7 pfu/ml was used for the functional characterization of AeStaufen. Blood viral titers were validated by plaque assay as described above. Mosquitoes were let to blood-feed for 1.5 h in the Hemotek membrane feeder system (Discovery Workshops) covered with porcine intestine (sausage casing). Fully engorged mosquitoes were selected and maintained in similar conditions as for the colony, with *ad libitum* access to water and 10 % sugar solution. Blood-feeding rate was calculated by dividing the number of engorged mosquitoes by the total number of mosquitoes that were offered the blood meals.

Survival rate was calculated at the collection time by dividing the number of living mosquitoes to the number of blood-fed mosquitoes.

RNA immunoprecipitation for AePur (AAEL012134) and AeStaufen (AAEL007470)

For AePur RIP, mosquitoes were orally infected by feeding them blood containing 10^7 PFU/ml DENV as described above. At 7 days post-infection (dpi), 10 mosquitoes were cold-anesthetized and homogenized in RIP lysis buffer [200 mM KCl, 20 mM HEPES pH7.2, 2% N-dodecyl-β-D -maltoside, 1% Igepal, 100 U/mL Murine RNase inhibitor (NEB)] using a bead mill homogenizer (FastPrep-24, MP Biomedicals). Homogenates were kept on ice for 30 min and centrifuged at 13,000 rpm for 15 min at 4℃. Cleared lysates were sonicated in an ultrasound bath cleaner (JP Selecta Ultrasons system, 40 kHz) for 15 sec and placed on ice for 15 sec. The sonication procedure was repeated three times.

To perform AeStaufen RIP, *AeStaufen* cDNA synthesized by Genscript was cloned into pIZT/ V5-His (Invitrogen). The same plasmid containing *Chloramphenicol acetyltransferase* (*CAT*) that was provided in the kit was used as expression control (Fig. S1A). Four µg of either plasmid were transfected into 6 x 10^5 C6/36 cells using TransIT-2020 transfection reagent (Mirus) for 4 h. After washing, cells were infected with DENV2 at multiplicity of infection (MOI) = 5. Two days post-infection, cells were collected in 150 µl of lysis buffer [200 mM KCl (Sigma), 20 mM HEPES (pH 7.2) (Sigma), 2 % N-dodecyl-β-D-maltoside (Thermo Fisher scientific), 1% Igepal CA-630 (Sigma), 100 U/mL Murine RNase inhibitor (NEB) and 1 X protease inhibitor cocktail (Roche)].

For RIP, 500 µg of protein lysate were diluted in 500 µl of NT2 buffer [50 mM Tris HCl (pH 7.4), 150 mM NaCl (Sigma), 1 mM $MgCl_2$ (Sigma), and 0.01% Igepal CA-630] and

534 incubated with 5 µg of rabbit anti-V5 antibody (Sigma), anti-Pur (Bethyl Laboratories), or
535 normal rabbit IgG (Merck) at 4 °C overnight. Bound complexes were captured into 50 µl of
536 Dynabeads-protein G (Thermo Fisher Scientific) by rotation for 2 h at 4 °C and washed four
537 times in NT2 buffer. Immunoprecipitates were analyzed by western blot and gRNA and sfRNA
538 were quantified by RT-qPCR.
539
540 **Western blot**
541 Immuno-precipitates or cells were lysed in RIPA lysis buffer (Cell Signaling Technology).
542 Proteins were separated under denaturing conditions on 4-15 % polyacrylamide gels (Bio-Rad)
543 and transferred onto polyvinylidene difluoride membranes (PVDF, Bio-Rad). The membranes
544 were blocked in 5 % slim milk (Bio-Rad), diluted in PBS-T (1st Base), at room temperature for
545 30 min, and incubated with 1: 5,000 rabbit anti-V5 (Sigma), 1:1,000 rabbit anti-PurB (Bethyl
546 Laboratories), 1:2,000 rat anti-PurA/PurB (kind gift from Robert Kelm, University of
547 Vermont), 1:10,000 mouse anti-Actin (MA5-11869, Thermo Fisher Scientific) or 1:1,000 anti-
548 GAPDH antibodies at 4 °C overnight. The blots were washed three times with PBS-T buffer,
549 incubated with goat anti-rabbit HRP, goat anti-mouse HRP or goat anti-rat HRP (Jackson
550 ImmunoResearch) at room temperature for 1 h. After three PBS-T washes, blots were
551 visualized using chemiluminescence imaging system (Bio-Rad) with SuperSignal West
552 (Thermo Fisher Scientific).
553
554 **Quantification of sfRNA and gRNA copies by real-time RT-qPCR**
555 Mosquito tissues were homogenized in 350 µl of TRK lysis buffer [E.Z.N.A. Total RNA kit I
556 (OMEGA Bio-Tek)] with silica beads (BioSpec) using mini-beadbeater (BioSpec). Saliva-

557 containing mixture and cells were lysed in 350 µl of TRK lysis buffer without bead
558 homogenization. Total RNA was extracted using the E.Z.N.A. Total RNA kit I protocol and
559 eluted with 30 µl DEPC-treated water (Ambion).

560 gRNA was quantified by RT-qPCR using the iTaq Universal probe one-step kit (Bio-Rad)
561 with primers and probe targeting the DENV2 envelope [27]. The 12.5 µl reaction mix contained
562 400 nM of forward and reverse primers, 200 nM of probe and 4 µl of RNA extract. sfRNA and
563 3'UTR were quantified together by RT-qPCR using the iTaq Universal Sybr green one-step kit
564 (Bio-Rad) with primers previously designed [26]. The 10 µl reaction mix contained 300 nM of
565 forward and reverse primers and 4 µl of RNA extract. Quantification was conducted with a
566 CFX96 Touch Real-Time PCR Detection System (Bio-Rad). The thermal profile for gRNA
567 quantification was 50 °C for 10 min, 95 °C for 1 min and 40 cycles of 95 °C for 10 sec and 60
568 °C for 15 sec, while that for sfRNA1/3'UTR quantification was 50 °C for 20 min, 95 °C for 1
569 min and 40 cycles of 95 °C for 10 sec and 60 °C for 15 sec, followed by melting curve analysis.

570 To absolutely quantify gRNA and sfRNA/3'UTR, we amplified templates encompassing
571 either the gRNA or the sfRNA/3'UTR targets using forward T7-tagged primers; for gRNA we
572 used 5'-CAGGATAAGAGGTTCGTCTG-3' and 5'-TTGACTCTTGTTTATCCGCT-3',
573 resulting in a 453 bp fragment; for sfRNA we used 5'-AGAAGAGGAAGAGGCAGGA-3' and
574 5'-CATTGTTGCTGCGATTTGT-3', resulting in a 319 bp fragment. Templates were
575 transcribed using the MegaScript T7 kit and purified using the E.Z.N.A total RNA extraction
576 kit. As we did not treat the template samples with DNase, there may be some DNA left after
577 RNA purification. Both DNA and RNA were simultaneously quantified at 260 nm absorbance
578 using a NanoDrop 2000 spectrophotometer (ThermoFisher Scientific). Dilutions of specific
579 quantities of RNA fragments were used to generate absolute standard curves.

580 sfRNA copy number was calculated by subtracting the number of gRNA fragments
581 (estimated using the envelope primers) from the combined number of sfRNA and 3'UTR
582 copies (estimated using the 3'UTR/ sfRNA1 primers). For infected samples that contained
583 detectable amount of sfRNA, sfRNA: gRNA ratio was calculated by dividing the number of
584 sfRNAs over the number of gRNAs.
585
586 **Double-stranded RNA-mediated RNAi**
587 The DNA templates used to generate dsRNA against the 14 3'UTR-interacting proteins were
588 synthesized using T7-tagged primer pairs as detailed in Table S3. A size-matched fragment
589 from *E. coli LacZ* was used as the template for generating dsRNA control (dsCtl). The PCR
590 fragments were transcribed using the MegaScript T7 transcription kit and the resulting dsRNA
591 was purified using the E.Z.N.A. Total RNA kit I (Omega) and folded by heating to 95°C for 2
592 min and slowly cooling down at 0.1 °C per second using a thermocycler (Bio-Rad). DsRNA
593 concentrations were adjusted to 3 or 14 µg / µl using SpeedVac Concentrator (Thermo
594 Scientific) and their integrity was checked on agarose gels. The dsRNA was then injected into
595 the thorax of two- to four-day-old cold-anesthetized female mosquitoes. 69 nl of 3 µg / µl
596 dsRNA was used for functional evaluation of the 14 3'UTR-interacting proteins in whole
597 mosquitoes and 138 nl of 14 µg / µl of AeStaufen dsRNA was used for functional evaluation
598 of AeStaufen in different tissues, including the salivary glands. The same amounts of dsLacZ
599 were injected as control in both experiments.
600
601 **Gene expression quantification**

Total RNA was extracted from 10 mosquitoes or 10 organs using the E.Z.N.A. Total RNA kit I, DNase-treated using the TURBO DNA-free kit (Thermo Fisher Scientific) and reverse-transcribed using the iScript cDNA Synthesis Kit (Bio-Rad). Gene expression was quantified using the SensiFAST SYBR No-ROX Kit (Bioline) with the primers listed in Table S4. The mRNA levels of *Actin*, a house-keeping gene, was quantified to normalize mRNA amount. Quantification was conducted on a CFX96 Touch Real-Time PCR Detection System with the following thermal profile: 95°C for 1 min and 40 cycles of 95 °C for 10 sec and 60 °C for 15 sec, followed by melting curve analysis. Three repeats were conducted.

Quantification of focus forming units

Single whole mosquitoes were homogenized in 500 µl of RPMI medium with silica beads (BioSpec) using mini-beadbeater (BioSpec). Homogenized tissues and saliva were sterilized by passing them through 0.22 µm filter (Sartorius). Samples were subjected to a 10-fold serial dilution in RPMI medium and 150 µl of each dilution was incubated with 1.5 x 10^5 C6/36 cells for 1 h, with gentle rocking at every 15 min. The inoculum was then removed and 1 ml of 1 % carboxymethyl cellulose (CMC) (Aquacide II, Calbiochem) and 2% FBS diluted in RPMI medium was added. After 3 days, the CMC medium was removed and the cells were fixed with 4 % paraformaldehyde (Merck), permeabilized with 0.5 % Triton X-100 (Sigma), blocked with 2% FBS, and stained using 1:400 mouse monoclonal anti-envelope antibody (4G2) and 1:20,000 secondary anti-mouse Dylight 680 (Rockland). Focus forming units (ffu) were counted using the Odyssey Clx imaging system (LI-COR) in three replicates per dilution and the average ffu per sample was calculated. Infection rate corresponded to the number of samples with at least one ffu over the total number of tested samples.

625

626 **siRNA-mediated gene silencing**

627 The siRNAs targeting HsPURA [SI00696066 (A1), SI04175367 (A2) and SI04342744 (A3)]
628 and siRNAs targeting HsPURB [SI04176879 (B1), SI04357661 (B2), SI04376281(B9)] were
629 obtained from Qiagen. The siRNA negative control (siNC) ON-TARGETplus siRNA#2 was
630 obtained from Dharmacon (Horizon Discovery). A final concentration of 5 nM siRNA was
631 complexed with 2.5 µl of Lipofectamine RNAiMax (Invitrogen) and incubated in 12-well
632 plates for 15 minutes prior to the plating of 1.3 x 10^5 Huh7 cells. Forty-eight hours post-
633 transfection, cells were infected with DENV NGC at a MOI of 0.1. At 24 hours post-infection
634 (hpi) plaque assay was performed on the supernatant as previously detailed [27], and at 48 hpi,
635 western blot analysis was conducted on cell lysates.

636

637 **CRISPR/Cas9-mediated knockout**

638 Two short-guide RNAs (sgRNA) targeting the sequences 5'-
639 CGAGCAGGGTGGTGCGGCGC-3' and 5-CGGCGGCGAGCAAGAGACGC-3'
640 corresponding to *HsPURA* and *HsPURB*, respectively, were designed with an online CRISPR
641 tool (crispr.mit.edu). The sgRNAs were cloned into pSpCas9-BB-2A-GFP (Adgene) as
642 previously detailed [63]. 2.3 x 10^5 Huh-7 cells were transfected with 2 µg of pSpCas9-BB-2A-
643 GFP-sgPURA using Lipofectamine 2000 (Invitrogen) following the manufacturer's
644 instructions. At 24 h post-transfection, cells expressing GFP were sorted on a BD FACSAria
645 II flow cytometer (BD Biosciences) and single cells were isolated by serial dilution to generate
646 clonal populations of HsPURA knockout (KO) cells. HsPurA depletion was validated using
647 western blotting. One of the PURA KO clones was then transfected with pSpCas9-BB-2A-

GFP-sgPURB following the same procedure as for generating HsPurA KO. Four double HsPURA/HsPURB KO clones were produced. PURA/B KO cells were infected as detailed for siRNA-silenced cells.

Intrathoracic inoculation

Four days post-injection of dsRNA against *AeStaufen*, 0.035 pfu of DENV2 were inoculated into the thorax of individual female mosquitoes using Nanoject II (Drummond scientific company). Mosquitoes were analyzed 7 days post-inoculation, assuming a similar incubation period as that of 10 days post-oral infection, as the midgut stage is bypassed during intrathoracic inoculation.

Saliva collection

At seven days post-inoculation or ten days post-oral infection, mosquitoes were immobilized by cutting their wings and legs and their proboscises were inserted individually into 20 µl tips, containing 10 µl of equal volume of RPMI medium and SPF pig blood. After 30 min, mosquitoes were visually observed for the presence of blood in their abdomen. To prevent false negatives, we analyzed saliva only from mosquitoes in which blood could be visually detected, indicating feeding and, hence, salivation. Salivation rate was calculated by dividing the number of salivating mosquitoes over the number of living mosquitoes.

Statistics

669 Z-test, unpaired T-test, and Dunnett's test were conducted with Prism 8.0.2 (GraphPad). Copies
670 of gRNA and titers (FFU) were log-transformed before statistical analysis to meet normal
671 distribution.
672
673 **Acknowledgement**
674 We are very thankful to Mariano Garcia-Blanco from University of Texas Medical Branch
675 (UTMB) for his support. We thank members of the Garcia-Blanco-Pompon Laboratory (Duke-
676 NUS) for their important suggestions and support. We also thank the scientific editor
677 Ravinuthula Sruthi Jagannathan for editing. Funding for this research came from a National
678 Medical Research Council ZRRF grant (ZRRF/007/2017) and a French Agence Nationale de
679 la Recherche grant (ANR-20-CE15-0006) both awarded to JP, a Rubicon scholarship from the
680 Dutch Research Council (NOW) awarded to MD and the Emerging Infectious Diseases (EID)
681 Signature Research Programme at Duke-NUS funded by the Agency for Science Technology
682 and Research (A*STAR). We thank the Mass Spectrometry Facility at UTMB, partially
683 supported by the Cancer Prevention Research Institute of Texas (CPRIT RP190682).
684

Bibliography

1. Gubler DJ. Cities spawn epidemic dengue viruses. Natural Medicines. 2004;10: 129–130. doi:10.1038/nm0204-129

2. Pierson TC, Diamond MS. The continued threat of emerging flaviviruses. Nature Microbiology. 2020;5: 796–812. doi:10.1038/s41564-020-0714-0

3. Bhatt S, Gething PW, Brady OJ, Messina JP, Farlow AW, Maoyes CL, et al. The global distribution and burden of dengue. Nature. 2013;496: 504–507. doi:10.1038/nature12060

4. Kraemer MUG, Reiner RC, Brady OJ, Messina JP, Gilbert M, Pigott DM, et al. Past and future spread of the arbovirus vectors Aedes aegypti and Aedes albopictus. Nature Microbiology. 2019; 1. doi:10.1038/s41564-019-0376-y

5. Thomas SJ, Yoon I-K. A review of Dengvaxia®: development to deployment. Human Vaccines & Immunotherapeutics. 2019;15: 2295–2314. doi:10.1080/21645515.2019.1658503

6. Ooi E-E, Goh K-T, Gubler DJ. Dengue prevention and 35 years of vector control in Singapore. Emerging Infectious Diseases. 2006;12: 887–893. doi:10.3201/10.3201/eid1206.051210

7. Barrows NJ, Campos RK, Liao K-C, Prasanth KR, Soto-Acosta R, Yeh S-C, et al. Biochemistry and Molecular Biology of Flaviviruses. Chem Rev. 2018;118: 4448–4482. doi:10.1021/acs.chemrev.7b00719

8. Diosa-Toro M, Prasanth KR, Bradrick SS, Garcia Blanco MA. Role of RNA-binding proteins during the late stages of Flavivirus replication cycle. Virol J. 2020;17: 60. doi:10.1186/s12985-020-01329-7

9. Mazeaud C, Freppel W, Chatel-Chaix L. The Multiples Fates of the Flavivirus RNA Genome During Pathogenesis. Front Genet. 2018;9: 595. doi:10.3389/fgene.2018.00595

10. Phillips SL, Soderblom EJ, Bradrick SS, Garcia-Blanco MA. Identification of Proteins Bound to Dengue Viral RNA In Vivo Reveals New Host Proteins Important for Virus Replication. mBio. 2016;7: e01865-15. doi:10.1128/mBio.01865-15

11. Ooi YS, Majzoub K, Flynn RA, Mata MA, Diep J, Li JK, et al. An RNA-centric dissection of host complexes controlling flavivirus infection. Nat Microbiol. 2019; 1–14. doi:10.1038/s41564-019-0518-2

12. Viktorovskaya OV, Greco TM, Cristea IM, Thompson SR. Identification of RNA Binding Proteins Associated with Dengue Virus RNA in Infected Cells Reveals Temporally Distinct Host Factor Requirements. PLOS Neglected Tropical Diseases. 2016;10: e0004921. doi:10.1371/journal.pntd.0004921

13. Gomila RC, Martin GW, Gehrke L. NF90 binds the dengue virus RNA 3' terminus and is a positive regulator of dengue virus replication. PLoS One. 2011;6: e16687. doi:10.1371/journal.pone.0016687

14. Anwar A, Leong KM, Ng ML, Chu JJH, Garcia-Blanco MA. The polypyrimidine tract-binding protein is required for efficient dengue virus propagation and associates with the viral replication machinery. J Biol Chem. 2009;284: 17021–17029. doi:10.1074/jbc.M109.006239

15. Lei Y, Huang Y, Zhang H, Yu L, Zhang M, Dayton A. Functional interaction between cellular p100 and the dengue virus 3' UTR. J Gen Virol. 2011;92: 796–806. doi:10.1099/vir.0.028597-0

16. Ward AM, Calvert MEK, Read LR, Kang S, Levitt BE, Dimopoulos G, et al. The Golgi associated ERI3 is a Flavivirus host factor. Sci Rep. 2016;6: 34379. doi:10.1038/srep34379

17. Dong Y, Yang J, Ye W, Wang Y, Miao Y, Ding T, et al. LSm1 binds to the Dengue virus RNA 3' UTR and is a positive regulator of Dengue virus replication. International Journal of Molecular Medicine. 2015;35: 1683–1689. doi:10.3892/ijmm.2015.2169

18. Ward AM, Bidet K, Yinglin A, Ler SG, Hogue K, Blackstock W, et al. Quantitative mass spectrometry of DENV-2 RNA-interacting proteins reveals that the DEAD-box RNA helicase DDX6 binds the DB1 and DB2 3' UTR structures. RNA Biol. 2011;8: 1173–1186. doi:10.4161/rna.8.6.17836

19. Polacek C, Friebe P, Harris E. Poly(A)-binding protein binds to the non-polyadenylated 3' untranslated region of dengue virus and modulates translation efficiency. Journal of General Virology,. 2009;90: 687–692. doi:10.1099/vir.0.007021-0

738 20. Diosa-Toro M, Kennedy DR, Chuo V, Popov VL, Pompon J, Garcia-Blanco MA. Y-Box Binding
739 Protein 1 Interacts with Dengue Virus Nucleocapsid and Mediates Viral Assembly. mBio.
740 2022;13: e00196-22.

741 21. Liao K-C, Chuo V, Ng WC, Neo SP, Pompon J, Gunaratne J, et al. Identification and
742 Characterization of Host Proteins Bound to Dengue Virus 3'UTR Reveal an Anti-viral Role for
743 Quaking Proteins. RNA. 2018; rna.064006.117. doi:10.1261/rna.064006.117

744 22. Pijlman GP, Funk A, Kondratieva N, Leung J, Torres S, van der Aa L, et al. A highly structured,
745 nuclease-resistant, noncoding RNA produced by flaviviruses is required for pathogenicity. Cell
746 Host & Microbe. 2008;4: 579–591. doi:10.1016/j.chom.2008.10.007

747 23. MacFadden A, O'Donoghue Z, Silva PAGC, Chapman EG, Olsthoorn RC, Sterken MG, et al.
748 Mechanism and structural diversity of exoribonuclease-resistant RNA structures in flaviviral
749 RNAs. Nature Communications. 2018;9: 119. doi:10.1038/s41467-017-02604-y

750 24. Slonchak A, Khromykh AA. Subgenomic flaviviral RNAs: What do we know after the first decade
751 of research. Antiviral Research. 2018 [cited 18 Sep 2018]. doi:10.1016/j.antiviral.2018.09.006

752 25. Manokaran G, Finol E, Wang C, Gunaratne J, Bahl J, Ong EZ, et al. Dengue subgenomic RNA binds
753 TRIM25 to inhibit interferon expression for epidemiological fitness. Science. 2015;350: 217–221.
754 doi:10.1126/science.aab3369

755 26. Bidet K, Dadlani D, Garcia-Blanco MA. G3BP1, G3BP2 and CAPRIN1 are required for translation
756 of interferon stimulated mRNAs and are targeted by a dengue virus non-coding RNA. PloS
757 Pathogens. 2014;10: e1004242. doi:10.1371/journal.ppat.1004242

758 27. Pompon J, Manuel M, Ng GK, Wong B, Shan C, Manokaran G, et al. Dengue subgenomic flaviviral
759 RNA disrupts immunity in mosquito salivary glands to increase virus transmission. PLoS
760 Pathogens. 2017;13: e1006535. doi:10.1371/journal.ppat.1006535

761 28. Yeh S-C, Tan WL, Chowdhury A, Chuo V, Kini RM, Pompon* J, et al. The anti-immune dengue
762 subgenomic flaviviral RNA is found in vesicles in mosquito saliva and associates with increased
763 infectivity. bioRxiv. 2021; 2021.03.02.433543. doi:10.1101/2021.03.02.433543

764 29. Barletta A, Silva MCLN, Sorgine M. Validation of Aedes aegypti Aag-2 cells as a model for insect
765 immune studies. Parasites & Vectors. 2012;5: 148.

766 30. Lv M, Yao Y, Li F, Xu L, Yang L, Gong Q, et al. Structural insights reveal the specific recognition of
767 roX RNA by the dsRNA-binding domains of the RNA helicase MLE and its indispensable role in
768 dosage compensation in Drosophila. Nucleic Acids Research. 2019;47: 3142–3157.
769 doi:10.1093/nar/gky1308

770 31. Moschall R, Rass M, Rossbach O, Lehmann G, Kullmann L, Eichner N, et al. Drosophila Sister-of-
771 Sex-lethal reinforces a male-specific gene expression pattern by controlling Sex-lethal
772 alternative splicing. Nucleic Acids Research. 2019;47: 2276–2288. doi:10.1093/nar/gky1284

773 32. Park E, Maquat LE. Staufen-mediated mRNA decay. Wiley interdisciplinary reviews RNA. 2013;4:
774 423–435. doi:10.1002/wrna.1168

775 33. Cesario J, McKim KS. RanGTP is required for meiotic spindle organization and the initiation of
776 embryonic development in Drosophila. Journal of Cell Science. 2011;124: 3797–3810.
777 doi:10.1242/jcs.084855

778 34. Zhang Q, Zhang L, Gao X, Qi S, Chang Z, Wu Q. DIP1 plays an antiviral role against DCV infection
779 in Drosophila melanogaster. Biochemical and Biophysical Research Communications. 2015;460:
780 222–226.

781 35. Sanghavi P, Liu G, Veeranan-Karmegam R, Navarro C, Gonsalvez GB. Multiple Roles for
782 Egalitarian in Polarization of the Drosophila Egg Chamber. Genetics. 2016;203: 415–432.
783 doi:10.1534/genetics.115.184622

784 36. Gerlach JM, Furrer M, Gallant M, Birkel D, Baluapuri A, Wolf E, et al. PAF1 complex component
785 Leo1 helps recruit Drosophila Myc to promoters. PNAS. 2017;114: E9224–E9232.
786 doi:10.1073/pnas.1705816114

787 37. Weber J, Bao H, Hartlmüller C, Wang Z, Windhager A, Janowski R, et al. Structural basis of
788 nucleic-acid recognition and double-strand unwinding by the essential neuronal protein Pur-
789 alpha. eLife Sciences. 2016;5: e11297. doi:10.7554/eLife.11297

790 38. Daniel DC, Johnson EM. PURA, the gene encoding Pur-alpha, member of an ancient nucleic acid-
791 binding protein family with mammalian neurological functions. Gene. 2018;643: 133–143.
792 doi:10.1016/j.gene.2017.12.004

793 39. White LA. Susceptibility of Aedes albopictus C6/36 cells to viral infection. J Clin Microbiol.
794 1987;25: 1221–1224. doi:10.1128/jcm.25.7.1221-1224.1987

795 40. Vaughn DW, Green S, Kalayanarooj S, Innis BL, Nimmannitya S, Suntayakorn S, et al. Dengue
796 viremia titer, antibody response pattern, and virus serotype correlate with disease severity. The
797 Journal of Infectious Diseases. 2000;181: 2–9. doi:10.1086/315215

798 41. Lambrechts L, Paaijmans KP, Fansiri T, Carrington LB, Kramer LD, Thomas MB, et al. Impact of
799 daily temperature fluctuations on dengue virus transmission by Aedes aegypti. PNAS. 2011;108:
800 7460–7465. doi:10.1073/pnas.1101377108

801 42. Stjohnston D, Beuchle D, Nussleinvolhard C. Staufen, a gene required to localize maternal RNAs
802 in the Drosophila egg. Cell. 1991;66: 51–63. doi:10.1016/0092-8674(91)90138-o

803 43. Liao K-C, Chuo V, Fagg WS, Bradrick SS, Pompon J, Garcia-Blanco MA. The RNA binding protein
804 Quaking represses host interferon response by downregulating MAVS. RNA Biology. 2019;0: 1–
805 15. doi:10.1080/15476286.2019.1703069

806 44. Dasso M. Running on Ran: Nuclear Transport and the Mitotic Spindle. Cell. 2001;104: 321–324.
807 doi:10.1016/S0092-8674(01)00218-5

808 45. Ye T, Zhang X. Involvement of Ran in the regulation of phagocytosis against virus infection in S2
809 cells. Developmental & Comparative Immunology. 2013;41: 491–497.
810 doi:10.1016/j.dci.2013.07.015

811 46. Ge M, Zhang T, Zhang M, Cheng L. Ran participates in deltamethrin stress through regulating the
812 nuclear import of Nrf2. Gene. 2021;769: 145213. doi:10.1016/j.gene.2020.145213

813 47. Dienstbier M, Boehl F, Li X, Bullock SL. Egalitarian is a selective RNA-binding protein linking
814 mRNA localization signals to the dynein motor. Genes Dev. 2009;23: 1546–1558.
815 doi:10.1101/gad.531009

816 48. Mohr S, Kenny A, Lam STY, Morgan MB, Smibert CA, Lipshitz HD, et al. Opposing roles for
817 Egalitarian and Staufen in transport, anchoring and localization of oskar mRNA in the Drosophila
818 oocyte. PLOS Genetics. 2021;17: e1009500. doi:10.1371/journal.pgen.1009500

819 49. Marazzi I, Ho JSY, Kim J, Manicassamy B, Dewell S, Albrecht RA, et al. Suppression of the antiviral
820 response by an influenza histone mimic. Nature. 2012;483: 428–433. doi:10.1038/nature10892

50. Daigle JG, Krishnamurthy K, Ramesh N, Casci I, Monaghan J, McAvoy K, et al. Pur-alpha regulates cytoplasmic stress granule dynamics and ameliorates FUS toxicity. Acta neuropathologica. 2016;131: 605–620.

51. Basu M, Brinton MA. How do flavivirus-infected cells resist arsenite-induced stress granule formation? Future Virol. 2017;12: 247–249. doi:10.2217/fvl-2017-0033

52. Kim YK, Furic L, DesGroseillers L, Maquat LE. Mammalian Staufen1 recruits Upf1 to specific mRNA 3'UTRs so as to elicit mRNA decay. Cell. 2005;120: 195–208. doi:10.1016/j.cell.2004.11.050

53. Yeh S-C, Pompon J. Flaviviruses Produce a Subgenomic Flaviviral RNA That Enhances Mosquito Transmission. DNA Cell Biol. 2018;37: 154–159. doi:10.1089/dna.2017.4059

54. Huber RG, Lim XN, Ng WC, Sim AYL, Poh HX, Shen Y, et al. Structure mapping of dengue and Zika viruses reveals functional long-range interactions. Nature Communications. 2019;10: 1408. doi:10.1038/s41467-019-09391-8

55. Abrahamyan LG, Chatel-Chaix L, Ajamian L, Milev MP, Monette A, Clément J-F, et al. Novel Staufen1 ribonucleoproteins prevent formation of stress granules but favour encapsidation of HIV-1 genomic RNA. J Cell Sci. 2010;123: 369–383. doi:10.1242/jcs.055897

56. de Lucas S, Peredo J, Marión RM, Sánchez C, Ortín J. Human Staufen1 protein interacts with influenza virus ribonucleoproteins and is required for efficient virus multiplication. J Virol. 2010;84: 7603–7612. doi:10.1128/JVI.00504-10

57. Dixit U, Pandey AK, Mishra P, Sengupta A, Pandey VN. Staufen1 promotes HCV replication by inhibiting protein kinase R and transporting viral RNA to the site of translation and replication in the cells. Nucleic Acids Res. 2016;44: 5271–5287. doi:10.1093/nar/gkw312

58. Wada M, Lokugamage KG, Nakagawa K, Narayanan K, Makino S. Interplay between coronavirus, a cytoplasmic RNA virus, and nonsense-mediated mRNA decay pathway. PNAS. 2018;115: E10157–E10166. doi:10.1073/pnas.1811675115

59. Xie X, Zou J, Zhang X, Zhou Y, Routh AL, Kang C, et al. Dengue NS2A Protein Orchestrates Virus Assembly. Cell Host & Microbe. 2019;26: 606-622.e8. doi:10.1016/j.chom.2019.09.015

60. Apte-Sengupta S, Sirohi D, Kuhn RJ. Coupling of replication and assembly in flaviviruses. Current Opinion in Virology. 2014;9: 134–142. doi:10.1016/j.coviro.2014.09.020

61. Thomas MG, Tosar LJM, Loschi M, Pasquini JM, Correale J, Kindler S, et al. Staufen recruitment into stress granules does not affect early mRNA transport in oligodendrocytes. Molecular biology of the cell. 2005;16: 405–420.

62. Lemaitre B, Hoffmann J. The host defense of Drosophila melanogaster. Annual Review of Immunology. 2007;25: 697–743.

63. Ran FA, Hsu PD, Wright J, Agarwala V, Scott DA, Zhang F. Genome engineering using the CRISPR-Cas9 system. Nat Protoc. 2013;8: 2281–2308. doi:10.1038/nprot.2013.143

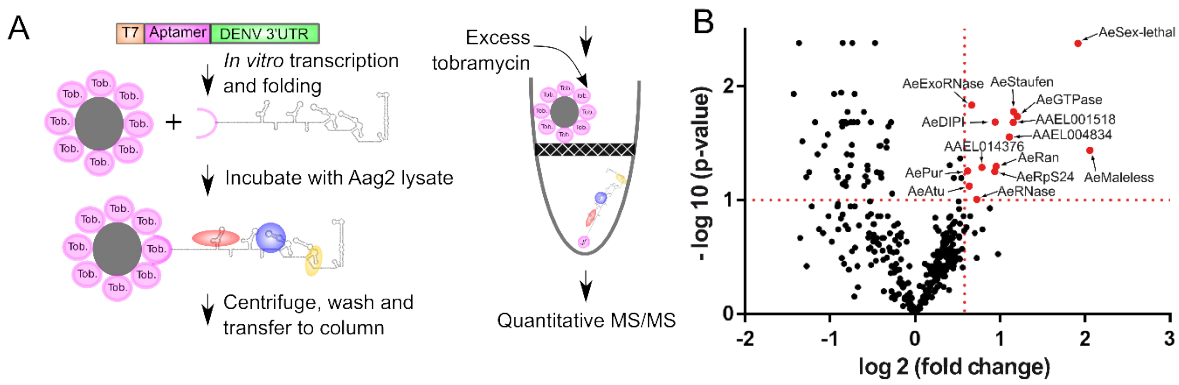

Figure 1. Application of RNA-affinity chromatography to identify *Aedes aegypti* proteins that interact with DENV2 3'UTR.

(A) Schematic of the RNA-affinity chromatography coupled with quantitative mass spectrometry (MS). **(B)** Identification of the DENV2 3'UTR-bound proteins. Of the 385 proteins detected, 14 interacted more than 1.5 fold ($p<0.1$) with DENV2 3'UTR, as compared to the control RNA. Interacting proteins are shown in red and their names are indicated with an arrow.

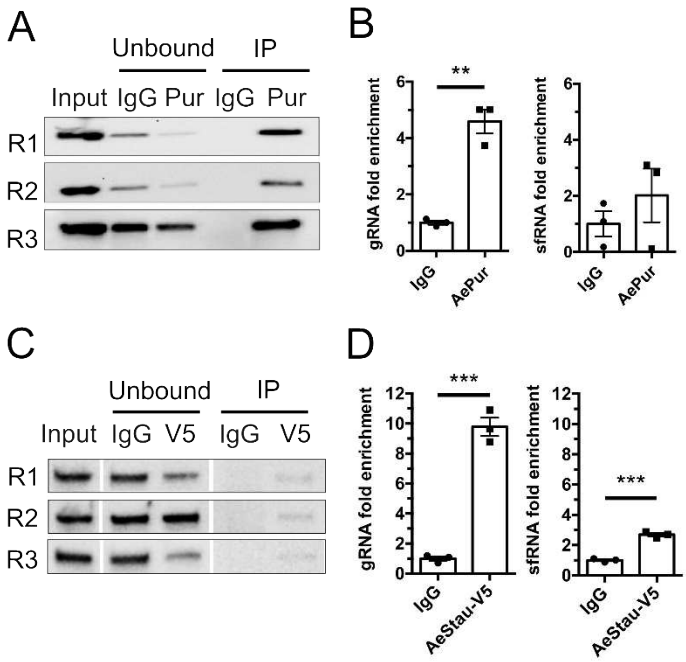

Figure 2. Binding affinities of AePur and AeStaufen to DENV2 3'UTR and sfRNA.

(A) Western blots of AePur immunoprecipitates from orally-infected mosquito lysates. **(B)** gRNA and sfRNA fold enrichments in AePur immunoprecipitates as compared to IgG control. **(C)** Western blots of AeStaufen-V5 (AeStau-V5) immunoprecipitates from infected C6/36 cell lysates. **(D)** gRNA and sfRNA fold enrichments in AeStaufen immunoprecipitates as compared to IgG control. (A, C) Three biological repeats (R1-3) are shown. (B, D) Bars show mean ± s.e.m. from three repeats. **, p-value < 0.01; ***, p-value < 0.001 as determined by unpaired T-test.

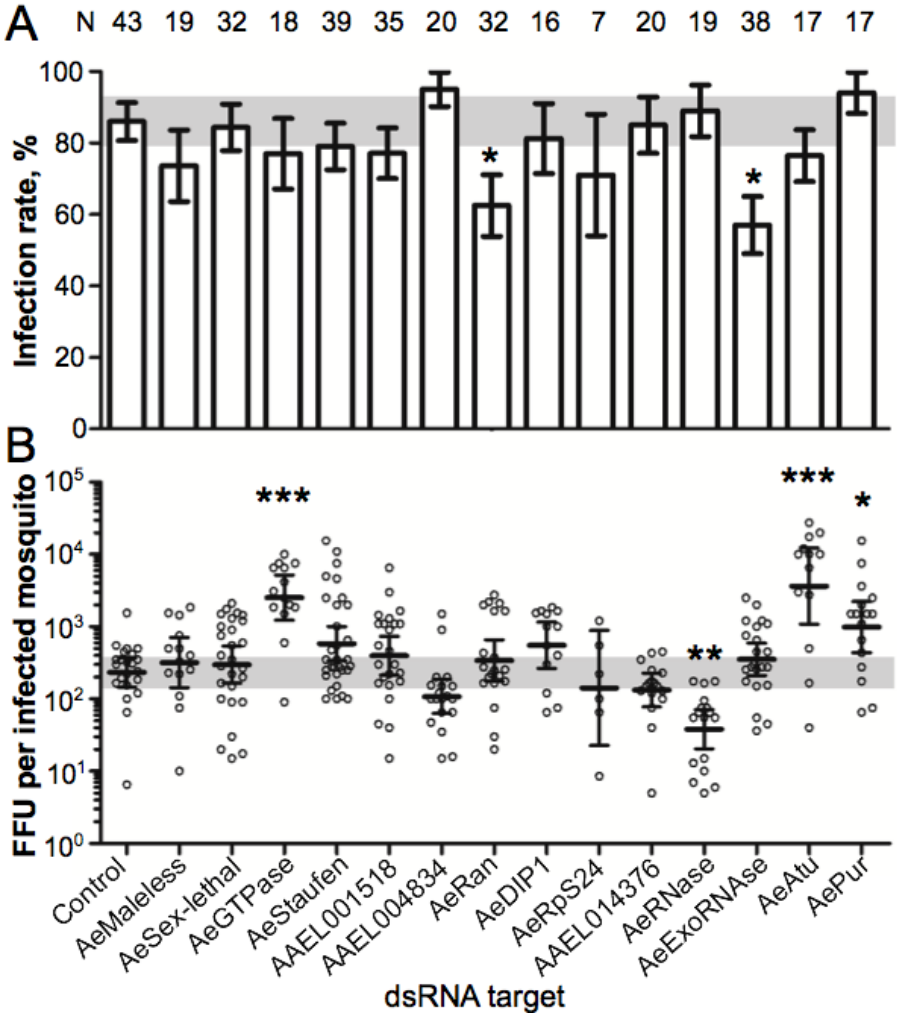

Figure 3. Effects of the 3'UTR-bound proteins on DENV infection in mosquitoes.

Four days post-dsRNA injection to silence each of the 14 3'UTR-bound proteins, mosquitoes were orally infected with 10^6 pfu/ml of DENV2. Infection was quantified 7 days later using focus forming unit (FFU) assay. **(A)** Infection rate. Bars show percentage ± s.e. *, p-value < 0.05 as determined by Z-test. **(B)** FFU per infected mosquito. Bars show geometric means ± 95% C.I. *, p-value < 0.05; ***, p-value < 0.001 as determined by Dunnett's test compared to control mosquitoes injected with dsRNA control. N, number of orally-infected mosquitoes. Data from three biological repeats, each using a specific set of dsRNA targets, were combined. DsRNA control was included in each repeat.

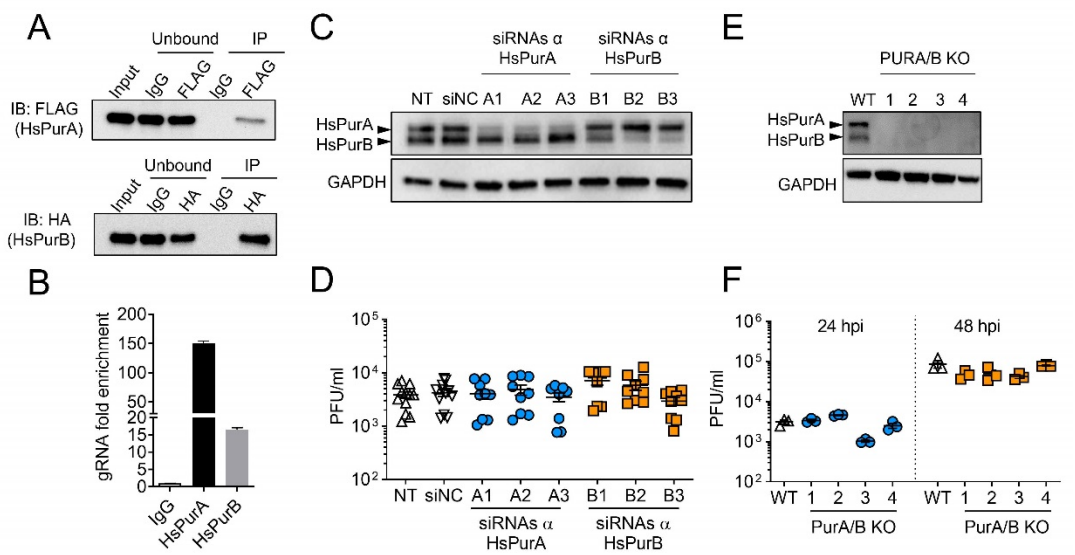

Figure 4. Human PurA and PurB interactions with DENV RNA and effect on infection in human cells.

(A) Western blots of FLAG-tagged HsPurA and HA-tagged HsPurB immunoprecipitates from Huh7 cells 24 hpi with DENV2 at a MOI of 5. **(B)** gRNA and sfRNA fold enrichments in FLAG-tagged HsPurA and HA-tagged HsPurB immunoprecipitates as compared to IgG control. Bars show mean ± s.e.m. from two repeats. **(C)** Western blots of HsPurA and HsPurB from cells silenced for either of the HsPUR proteins. Three different siRNAs were used for each protein. The picture is representative of multiple repeats. GAPDH was used as a loading control. **(D)** Effect of *HsPURA* or *HsPURB* silencing on viral load estimated by plaque forming unit (PFU) quantities in supernatants at 24 hpi with a MOI of 0.1. Bars indicate means ± s.e.m. **(E)** Western blots of HsPurA and HsPurB from cells, where both proteins were genetically-depleted. Four different double knock-out lines (PURA/B KO) for each protein were tested. The picture is representative of multiple repeats. GAPDH was used as a loading control. **(F)** Effect of HsPurA and HsPurB genetic ablation on viral loads estimated by PFU quantities in supernatants at 24 and 48hpi, with a MOI of 0.1. Bars indicate means ± s.e.m. NT, non-transfected control; siNC, transfected with control siRNA; WT, wild-type.

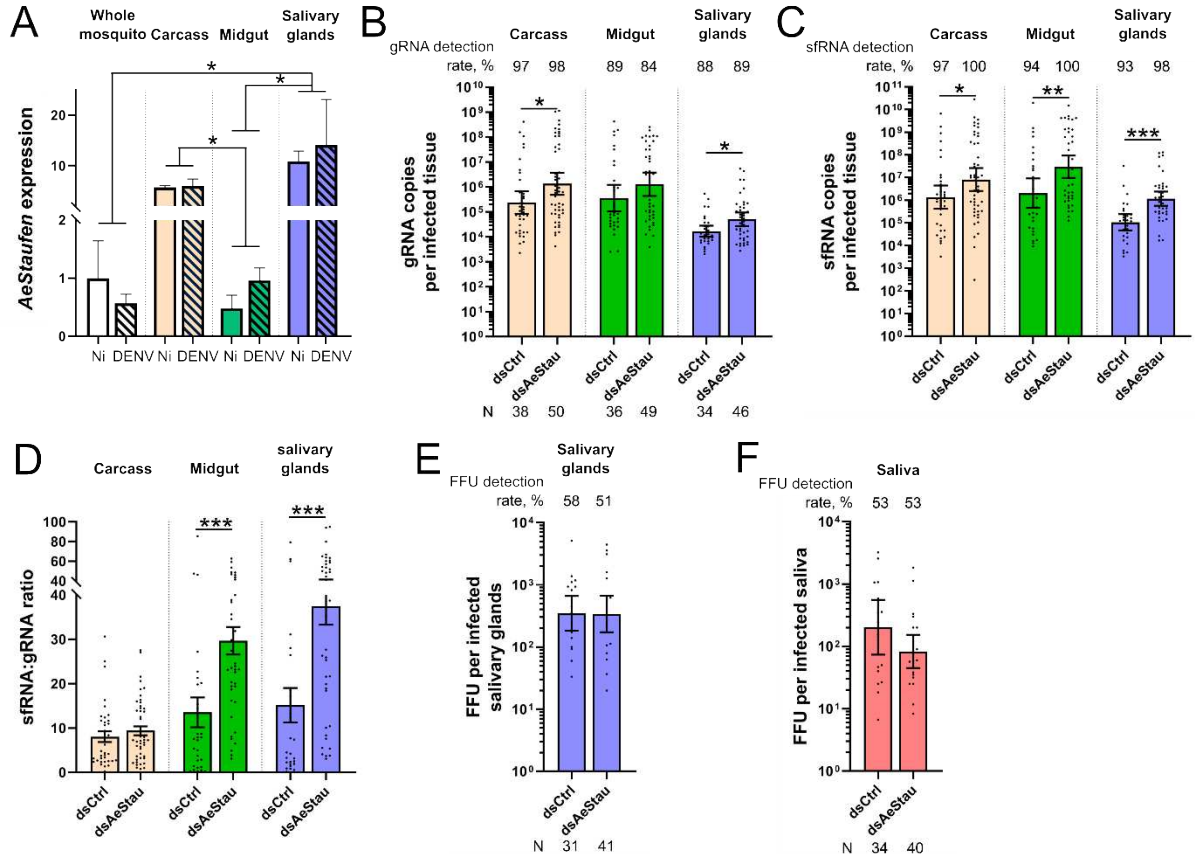

Figure 5. Effect of AeStaufen on gRNA and sfRNA copies, and viral titers in different mosquito tissues.

(A) *AeStaufen* relative expression in whole mosquitoes, carcass (what is left after dissection), midgut, and salivary glands at 10 days post non-infectious (Ni) or infectious blood-feeding (DENV). Bars represent means ± s.e.m. from three replicates of pools of ten tissues. **(B-D)** Effect of *AeStaufen* silencing (*dsAeStau*) on gRNA copies (B), sfRNA copies (C) and sfRNA:gRNA ratio (D) in the carcass, midgut and salivary glands at 10 days post-oral infection. **(E-F)** Effect *AeStaufen* silencing (*dsAeStau*) on viral titers as determined by focus forming unit (FFU) assay in salivary glands (E) and saliva (F) at 10 days post-oral infection. (B-F) *dsLacZ* was injected as control. (B, C, E, F) Bars indicate geometric means ± 95% C.I. (D) Bars indicate means ± s.e.m. N, number of mosquitoes analyzed. *, p-value < 0.05; **, p-value < 0.01; ***, p-value < 0.001 as determined by unpaired t-test or by LSD-Fisher test (A).

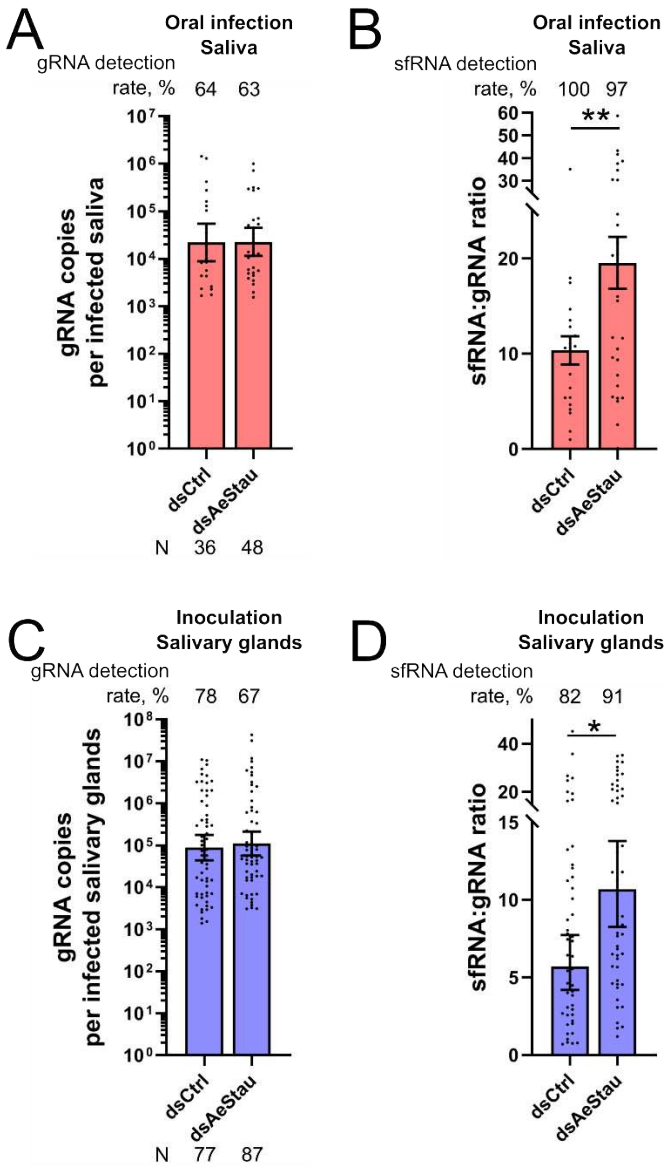

Figure 6. Effect of AeStaufen on sfRNA secretion in the saliva.

(A-B) Effect of *AeStaufen* silencing (*dsAeStau*) on gRNA copies (A) and sfRNA:gRNA ratio (B) in saliva collected at 10 days post-oral infection. **(C-D)** Effect of *AeStaufen* silencing (*dsAeStau*) on gRNA copies (C) and sfRNA:gRNA ratio (D) in the salivary glands at 7 days post-inoculation. *dsLacZ* was injected as control. (A, C) Bars indicate geometric means ± 95% C.I. (B, D) Bars indicate means ± s.e.m. N, number of mosquitoes analyzed. *, p-value < 0.05; **, p-value < 0.01 as determined by unpaired t-test.

Table 1. List of *A. aegypti* proteins that interact with DENV2 3'UTR and their corresponding human homologs. [1]Work carried out using RNA-affinity chromatography. [2]Human studies using RNA-affinity chromatography or ChIRP. [3]Cell type and viral fragments used are indicated.

Aedes aegypti			Human homolog	Fold changes in Human screens for flavivirus RNA-binding proteins[2,3]						
Aag2 – DENV2 3'UTR[1]				Huh7 – DENV2 5'+ 3' UTR (1)	Huh7 – DENV1 3'UTR (2)	Huh7 – DENV2 3'UTR (2)	Huh7 – DENV3 3'UTR (2)	Huh7 – DENV4 3'UTR (2)	Huh7 – DENV2 gRNA (3)	Huh7 – ZIKV gRNA [11]
Gene ID	Gene name	Fold change								
AAEL004859	AeMaleless	4.17	DHX9;		0 .55	0.54	0.34	0.65	3.43	2.48
			DHX29;							1.35
			DHX36;			1.30			1.46	1.78
			DHX57						1.39	1.61
AAEL011150	AeSex-lethal	3.78	ELAVL1; ELAVL2; ELAVL4; ELAVL3						2.8	2.20
AAEL003813	AeGTPase	2.30	MTG1							
AAEL019885	AeStaufen	2.24	STAU1		0.58	0.71	0.53	0.71	2.32	2.59
AAEL001518	AAEL001518	2.23	Not identified							
AAEL004834	AAEL004834	2.16	JADE3							
AAEL009287	AeRan	1.94	RAN	1.76					2.60	
AAEL012964	AeDIP1	1.92	ADARB1							
AAEL014292	AeRpS24	1.92	RpS24			0.68		0.57		
AAEL014376	AAEL014376	1.73	C3orf17							
AAEL001089	AeRNase	1.66	RPP14			1.22				
AAEL002463	AeExoRNase	1.59	EXD1							
AAEL006172	AeAtu	1.55	LEO1			1.22				
AAEL012134	AePur	1.54	PURB	1.94					2.04	

Table 1